Analysis of Inductive Dielectric Posts in Rectangular Waveguide

YEHUDA LEVIATAN, MEMBER, IEEE, AND GAD S. SHEAFFER

Abstract—**A rapidly converging moment solution for the complete analysis of homogeneous dielectric posts of the inductive type in rectangular waveguide is presented. The moment method approach uses filamentary currents to simulate both the field scattered by the post and the field inside the post and in turn point-matches the continuity conditions for the tangential components of the electric and magnetic fields across the post surface. The procedure is simple to execute and is general in that inductive posts of arbitrary smooth shape, size, location, and number, lossless as well as lossy, can be handled effectively. Data are given and compared with the few cases for which approximate results are available. The technique is further applied to other situations where no experimental data or other analytic results are available.**

I. INTRODUCTION

THE STUDY OF inductive waveguide posts has been a subject of interest to researchers for many years. Useful references to a portion of a large body of recent work with metallic posts are given in [1]. Dielectric posts, however, have attracted less attention, and the few treatments available deal exclusively with circular posts. Marcuvitz [2] has by variational method calculated the parameters of the equivalent circuit for a circular dielectric post discontinuity in a rectangular waveguide. The results were fairly accurate for dielectric posts of relatively thin diameter situated at the center of the waveguide, provided that neither of the equivalent circuit parameters was close to resonance. Nielsen [3] has overcome some of these limitations by developing a theory based upon the method of expanding the field in a sum of modes. His method, too, is applicable only to circular centered posts but is extended to posts of any size and complex permittivity. Nielsen also improved the results near resonance. Recently, Araneta *et al.* [4] presented a higher order variational model for centrally placed dielectric rod of circular cross section. Their model has no restrictions on the rod diameter, and it also shows an improved representation near resonance. A subsequent paper by Sahalos and Vafiadis [5] suggested a procedure similar to that given by Nielsen [3] using a circular rather than rectangular interaction region. Their model permits the analysis of circular posts in the middle of a rectangular waveguide and renders the results near resonance very accurate. The main purpose of this paper is to devise a procedure which is accurate, simple, and general in that inductive posts, lossless as well as lossy, of arbitrary smooth shape, size, location, and number can be handled effectively. The study of dielectric posts is not solely of academic interest; it has practical importance as well. Nowadays, several high-permittivity, high-Q, temperature-stable, low-cost ceramic compositions have been developed. With this combination of desirable properties, they can replace conventional copper and Invar waveguide filters in almost all applications. In fact, dielectric filters have already been used in radio system ranging from 1.7 to 11 GHz, and their application is expected to grow rapidly in the future [6].

A short while ago, the problem of electromagnetic scattering by perfectly conducting inductive posts in rectangular waveguide was facilitated via an efficient and fairly simple moment solution [7], [8]. The suggested idea is to use a filamentary current as an approximate current source producing the field scattered by the post and a point-matching procedure for the boundary condition at the post surface. Specifically, the post is replaced by a set of unknown current filaments placed on or inside the post surface, the latter being usually preferable since it yields a more rapidly converging numerical solution. A point-matching of the boundary condition at the post surface is imposed and the unknown current filaments are determined. These currents in turn are used to evaluate other subjects of interest, such as the equivalent circuit parameters and the actual surface-induced current.

In this paper, attention is focused on the class of dielectric inductive posts. The basic formulation introduced deals exclusively with a single inductive dielectric post. The formulation for structures that seem to be more complicated, such as the post array, requires only trivial modification of the basic one and, for the sake of brevity, is not presented in the following analytical exposition. Our main objective is to extend the above-described analysis to handle homogeneous dielectric inductive posts using a multifilament current model. In treating inductive dielectric posts, one option is to utilize the standard procedure, which expands the actual polarization current induced in the dielectric in terms of suitable basis functions and then point-matches the constitutive relationship at points inside the post. This approach, however, involves a Fredholm integral equation of the second kind in which the unknown current appears both under the integral sign and explicitly outside the integral sign. Therefore, filaments would not be suitable expansion functions if the point-matching proce-

Manuscript received April 28, 1986; revised August 12, 1986. This work was supported in part by the B. De Rothschild Foundation for the Advancement of Science in Israel, Inc.

The authors are with the Department of Electrical Engineering, Technion—Israel Institute of Technology, Haifa 32000, Israel.

IEEE Log Number 8611026.

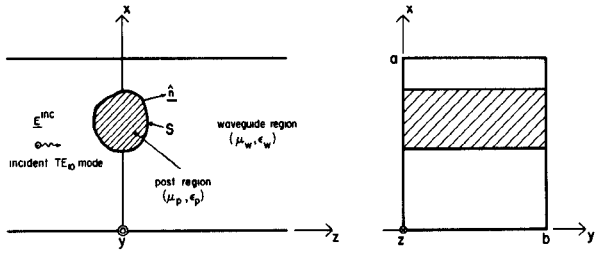

Fig. 1. Inductive dielectric post of arbitrary shape in a rectangular waveguide.

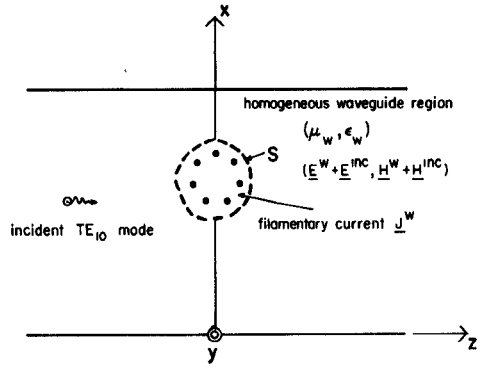

Fig. 2. Simulated equivalence for region W.

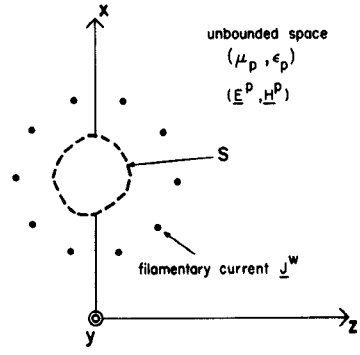

Fig. 3. Simulated equivalence for region P.

dure is to be used for testing. In this case, one may expand the polarization current in terms of pulse functions and use point matching for testing. As a matter of fact, this approach is currently being considered by Hsu and Auda [9]. Such a procedure, however, involves a volumetric integral equation which, in conjunction with the rather slowly converging Green's function, typically associated with waveguide discontinuity problems, would seriously tax the computing system. The other option is to employ two separate sets of filamentary currents as approximate current sources which simulate, respectively, the field scattered by the post and the field inside the post and then point-match the continuity conditions for the tangential components of both the electric and the magnetic field across the post surface. This latter approach seems to be more favorable and will be the one considered in this work.

II. Problem Specifications

The physical configuration of the problem under study is shown in Fig. 1, together with the coordinate system used. Here, we consider a cylindrical waveguide of rectangular cross section in which an inductive dielectric post is situated. The width of the guide is a and its height is b. The guide walls are perfect conductors and it is filled with a homogeneous medium of constitutive parameters μ_w and ϵ_w. The post is of arbitrary smooth cross section and is composed of homogeneous material with permeability $\mu_p = \mu_w$ and permittivity ϵ_p. Dissipation in the waveguide region is not accounted for; thus, μ_w and ϵ_w are considered real. For future convenience, we refer to the waveguide region external to the post as region W, to the post region as region P, and to the post surface as S.

The wave incident upon the post is the dominant TE_{10} mode traveling in the positive z direction. An $\exp(j\omega t)$ time dependence is assumed and suppressed. We confine our consideration to a frequency band within which the TE_{10} is the only propagating mode. Because the electric-field vector of the incident mode has only a y component, which is independent of y, and since the properties of the post, both physical and electrical, are uniform along the y direction, the total field in the waveguide does not vary with y. The problem thus reduces to a two-dimensional one.

Our main goal is to determine the field scattered by the post. By definition, the field scattered by the post is the actual field in the ambient waveguide region minus the incident field. Once the scattered field is known, a calculation of the scattering matrix and subsequently of the equivalent network parameters for the post two-port junction is straightforward.

III. Simulated Equivalent Situations

We now divide the original situation into two simulated equivalent situations. In the first situation, we simulate the electromagnetic field in the waveguide region W. In the second situation, we simulate the electromagnetic field in the post region P.

In the simulated equivalence for region W shown in Fig. 2, the post is replaced by a fictitious surface current distribution $\boldsymbol{J}^w$ placed on a closed surface enclosed in S. This current is y-directed and independent of the spatial y direction. $\boldsymbol{J}^w$ is treated as a source current in a homogeneous waveguide region filled with a medium of constitutive parameters μ_w and ϵ_w. In Fig. 2, $(\boldsymbol{E}^w, \boldsymbol{H}^w)$ is the electromagnetic field due to the current $\boldsymbol{J}^w$, and $(\boldsymbol{E}^{inc}, \boldsymbol{H}^{inc})$ is the electromagnetic field of the incident TE_{10} mode, both calculated with the post absent. The total field $(\boldsymbol{E}^w + \boldsymbol{E}^{inc}, \boldsymbol{H}^w + \boldsymbol{H}^{inc})$ in region W in the simulated equivalent situation for region W is simulating the field in region W in the original situation.

In the simulated equivalence for region P shown in Fig. 3, the waveguide region surrounding the post is replaced by a fictitious surface current distribution $\boldsymbol{J}^p$ placed on a closed surface enclosing S. This current is y-directed, infinite in extent in the y-direction, and independent of

the spatial y-direction. $\boldsymbol{J}^p$ is treated as a source current in an unbounded space filled with homogeneous material identical to that composing the post. The field $(\boldsymbol{E}^p, \boldsymbol{H}^p)$ in region P in the simulated equivalent situation for region P shown in Fig. 3 is simulating the field in region P in the original situation.

Note that in both Figs. 2 and 3, filamentary currents $\boldsymbol{J}^w$ and $\boldsymbol{J}^p$ are depicted, respectively. These are already particular choices of the approximations for $\boldsymbol{J}^w$ and $\boldsymbol{J}^p$ that will be introduced below and used thereafter.

The relationship between the electromagnetic fields $(\boldsymbol{E}^w + \boldsymbol{E}^{\text{inc}}, \boldsymbol{H}^w + \boldsymbol{H}^{\text{inc}})$ and $(\boldsymbol{E}^p, \boldsymbol{H}^p)$ in the simulated equivalent situation shown in Figs. 2 and 3, respectively, is dictated by the boundary condition at the post surface in the original problem shown in Fig. 1. Specifically, the tangential components of the electric and magnetic fields must be continuous across S. This leads to the operator equations

$$\hat{\boldsymbol{n}} \times (\boldsymbol{E}^w - \boldsymbol{E}^p) = -\hat{\boldsymbol{n}} \times \boldsymbol{E}^{\text{inc}} \quad \text{on } S \tag{1}$$

$$\hat{\boldsymbol{n}} \times (\boldsymbol{H}^w - \boldsymbol{H}^p) = -\hat{\boldsymbol{n}} \times \boldsymbol{H}^{\text{inc}} \quad \text{on } S \tag{2}$$

where $\hat{\boldsymbol{n}}$ is a unit vector normal to the post surface S and pointing towards the waveguide region, as shown in Fig. 1.

Evidently, if current distributions $\boldsymbol{J}^w$ and $\boldsymbol{J}^p$ were found which satisfy conditions (1) and (2), then $(\boldsymbol{E}^w, \boldsymbol{H}^w)$ would be the exact field scattered by the post and $(\boldsymbol{E}^p, \boldsymbol{H}^p)$ would be the exact field inside the post. With this goal in mind, $\boldsymbol{J}^w$ and $\boldsymbol{J}^p$ are first approximated by a finite number of expansion functions. Specifically $\boldsymbol{J}^w$ is approximated by a set of N^w y-directed filaments of yet unknown constant current $\{I_i^w\}$, $i = 1,2,\cdots,N^w$, situated on a contour inside S as shown in Fig. 2, and $\boldsymbol{J}^p$ is approximated by a set of N^p y-directed infinitely long filaments of yet unknown constant currents $\{I_i^p\}$, $i = 1,2,\cdots,N^p$, situated on a contour outside S as shown in Fig. 3. It is noteworthy that both the inner contour on which the $\{I_i^w\}$ are situated and the outer contour on which the $\{I_i^p\}$ are situated are arbitrary as far as the formulation is concerned. The question of selecting contours suitable for numerical computation will be discussed in Section V. Next, the two continuity conditions (1) and (2) are either strictly imposed at $N^s = \frac{1}{2}(N^w + N^p)$ selected points on S or are imposed, in the least-square-error sense, at $N^s > \frac{1}{2}(N^w + N^p)$ selected points on S. The result is a matrix equation which can be subsequently solved for $\{I_i^w\}$ and $\{I_i^p\}$. Once the currents are known, approximate values for the various fields and other parameters of interest can be readily found.

It should be remarked that from a strict mathematical point of view, we cannot, in general, guarantee the existence of current distributions $\boldsymbol{J}^w$ and $\boldsymbol{J}^p$ on arbitrarily selected inner and outer surfaces which produce the true fields in the respective regions. The existence question, which is an important one, is currently under investigation and will be reported in a forthcoming paper. For present purposes, suffice it to say that although (1) and (2) might not have a mathematically admissible solution for certain choices of inner and outer surfaces, they can nevertheless constitute a suitable formulation for a numerical solution. The reason for this is intimately related to the fact that the finite set of impulsive basis functions defined on the moved-away surfaces can be interpreted as a finite set of entire domain functions defined on S. In this sense, our basis is as appropriate as other entire-domain bases on S commonly employed in moment solutions for scattering problems. The advantage here lies in the representation of smooth quantities on S using impulsive sources whose fields are easily evaluated.

IV. Formulation

In this section, expressions for the various electromagnetic fields introduced in the preceding section are presented.

A. Expressions for $\boldsymbol{E}^{\text{inc}}$ and $\boldsymbol{H}^{\text{inc}}$

The incident electromagnetic field $(\boldsymbol{E}^{\text{inc}}, \boldsymbol{H}^{\text{inc}})$ is expressed as

$$\boldsymbol{E}^{\text{inc}} = \boldsymbol{u}_y E_y^{\text{inc}} \tag{3}$$

$$\boldsymbol{H}^{\text{inc}} = \boldsymbol{u}_x H_x^{\text{inc}} + \boldsymbol{u}_z H_z^{\text{inc}} \tag{4}$$

where

$$E_y^{\text{inc}} = \sin\frac{\pi x}{a} e^{-jk_{z1}z} \tag{5}$$

$$H_x^{\text{inc}} = -\frac{k_{z1}}{k_w \eta_w} \sin\frac{\pi x}{a} e^{-jk_{z1}z} \tag{6}$$

$$H_z^{\text{inc}} = -\frac{\pi}{jk_w \eta_w a} \cos\frac{\pi x}{a} e^{-jk_{z1}z}. \tag{7}$$

Here, $k_w = \omega\sqrt{\mu_w \epsilon_w}$ and $\eta_w = \sqrt{\mu_w/\epsilon_w}$ are, respectively, the wavenumber and intrinsic impedance in the waveguide region. Also, k_{z1} is the modal wavenumber of the propagating TE_{10} mode given by

$$k_{z1} = \sqrt{k_w^2 - \left(\frac{\pi}{a}\right)^2}. \tag{8}$$

B. Expressions for $\boldsymbol{E}^w$ and $\boldsymbol{H}^w$

The electromagnetic field $(\boldsymbol{E}^w, \boldsymbol{H}^w)$ due to the current filaments I_i^w, $i = 1,2,\cdots,N^w$, radiating in region w with the post absent is expressed as

$$\boldsymbol{E}^w = \boldsymbol{u}_y \sum_{i=1}^{N^w} E_{iy}^w \tag{9}$$

$$\boldsymbol{H}^w = \boldsymbol{u}_x \sum_{i=1}^{N^w} H_{ix}^w + \boldsymbol{u}_z \sum_{i=1}^{N^w} H_{iz}^w. \tag{10}$$

In (9)

$$E_{iy}^w = -\frac{k_w \eta_w I_i^w}{a} \sum_{m=1}^{\infty} \frac{1}{k_{zm}} \sin\frac{m\pi x_i^w}{a} \sin\frac{m\pi x}{a} e^{-jk_{zm}|z - z_i^w|} \tag{11}$$

is the intensity of the y-directed electric fields at observation point (x, z) in region W due to current filament I_i^w situated at (x_i^w, z_i^w). Here k_{zm} are the modal wavenumbers

given by

$$k_{zm} = -j\sqrt{\left(\frac{m\pi}{a}\right)^2 - k_w^2} \tag{12}$$

for $m \neq 1$ and by (8) for $m = 1$. Unfortunately, the series in (11) converges slowly and is therefore not convenient for computation. Following the approach outlined in [5], we convert it to

$$E_{iy} = S_{iy} + S_{iy}^{\text{aux}} \tag{13}$$

where S_{iy} is the rapidly convergent summation

$$S_{iy} = -\frac{k_w \eta_w I_i^w}{a} \sum_{m=1}^{\infty} \left(\frac{e^{-jk_{zm}|z-z_i^w|}}{k_{zm}} - \frac{e^{-(m\pi/a)|z-z_i^w|}}{-j\frac{m\pi}{a}} \right) \cdot \sin\frac{m\pi x_i^w}{a} \sin\frac{m\pi x}{a} \tag{14}$$

and S_{iy}^{aux} is the auxiliary series

$$S_{iy}^{\text{aux}} = -\frac{k_w \eta_w I_i^w}{a} \sum_{m=1}^{\infty} \frac{1}{-j\frac{m\pi}{a}} \sin\frac{m\pi x_i^w}{a} \cdot \sin\frac{m\pi x}{a} e^{-(m\pi/a)|z-z_i^w|} \tag{15}$$

that, when summed in closed form, reduces to

$$S_{iy}^{\text{aux}} = -\frac{jk_w \eta_w I_i^w}{2\pi} \operatorname{Re}\left\{ \ln\left(\frac{1-D_i}{1-C_i} \right) \right\} \tag{16}$$

with

$$C_i = \exp\left(j\frac{\pi}{a}\left[(x - x_i^w) + j|z - z_i^w| \right] \right) \tag{17}$$

$$D_i = \exp\left(j\frac{\pi}{a}\left[(x + x_i^w) + j|z - z_i^w| \right] \right). \tag{18}$$

In (10)

$$H_{ix}^w = \pm\frac{I_i^w}{a} \sum_{m=1}^{\infty} \sin\frac{m\pi x_i^w}{a} \sin\frac{m\pi x}{a} e^{-jk_{zm}|z-z_i^w|} \tag{19}$$

$$H_{iz}^w = \frac{I_i^w}{a} \sum_{m=1}^{\infty} \frac{m\pi}{jk_{zm}a} \sin\frac{m\pi x_i^w}{a} \cos\frac{m\pi x}{a} e^{-jk_{zm}|z-z_i^w|} \tag{20}$$

are the x and z components of the magnetic field at observation point (x, z) in region w due to current filament I_i^w situated at (x_i^w, z_i^w). The upper sign in (19) is for $z \geq z_i^w$ while the lower sign is for $z < z_i^w$. The series (19) and (20) are also slowly converging. Following the scheme outlined in [6], we convert them to

$$H_{ix}^w = S_{ix} + S_{ix}^{\text{aux}} \tag{21}$$

$$H_{iz}^w = S_{iz} + S_{iz}^{\text{aux}} \tag{22}$$

where S_{ix} and S_{iz} are the rapidly convergent summations

$$S_{ix} = \pm\frac{I_i^w}{a} \sum_{m=1}^{\infty} \left(e^{-jk_{zm}|z-z_i^w|} - e^{-(m\pi/a)|z-z_i^w|} \right) \cdot \sin\frac{m\pi x_i^w}{a} \sin\frac{m\pi x}{a} \tag{23}$$

and

$$S_{iz} = \frac{I_i^w}{a} \sum_{m=1}^{\infty} \left(\frac{m}{jk_{zm}a} e^{-jk_{zm}|z-z_i^w|} - e^{-(m\pi/a)|z-z_i^w|} \right) \cdot \sin\frac{m\pi x_i^w}{a} \cos\frac{m\pi x}{a}. \tag{24}$$

Here S_{ix}^{aux} and S_{iz}^{aux} are the two auxiliary series

$$S_{ix}^{\text{aux}} = \pm\frac{I_i^w}{a} \sum_{m=1}^{\infty} \sin\frac{m\pi x_i^w}{a} \sin\frac{m\pi x}{a} e^{-(m\pi/a)|z-z_i^w|} \tag{25}$$

$$S_{iz}^{\text{aux}} = \frac{I_i^w}{a} \sum_{m=1}^{\infty} \sin\frac{m\pi x_i^w}{a} \cos\frac{m\pi x}{a} e^{-(m\pi/a)|z-z_i^w|} \tag{26}$$

that, when summed in closed form, reduce to

$$S_{ix}^{\text{aux}} = \pm\frac{I_i^w}{2a} \operatorname{Re}\left\{ \frac{C_i - D_i}{(1-C_i)(1-D_i)} \right\} \tag{27}$$

$$S_{iz}^{\text{aux}} = \frac{I_i^w}{2a} \operatorname{Im}\left\{ \frac{D_i - C_i}{(1-C_i)(1-D_i)} \right\} \tag{28}$$

with C_i and D_i given, respectively, by (17) and (18).

C. Expressions for E^p and H^p

The electromagnetic field (E^p, H^p) due to the current filaments $I_i^p, i = 1, 2, \cdots, N^p$, radiating in an unbounded space of constitutive parameters μ_p and ϵ_p can be expressed as

$$E^p = u_y \sum_{i=1}^{N^p} E_{iy}^p \tag{29}$$

$$H^p = u_x \sum_{i=1}^{N^p} H_{ix}^p + u_z \sum_{i=1}^{N^p} H_{iz}^p. \tag{30}$$

In (29)

$$E_{iy}^p = -\frac{k_p \eta_p I_i^p}{4} H_0^{(2)}(k_p r_i^p) \tag{31}$$

is the intensity of the y-directed electric field at observation point (x, z) in region p due to current filament I_i^p situated at (x_i^p, z_i^p). Here, $k_p = \omega\sqrt{\mu_p \epsilon_p}$ and $\eta_p = \sqrt{\mu_p/\epsilon_p}$ are the wavenumber and intrinsic impedance, respectively, of the medium in region P. Also, $H_0^{(2)}$ is the Hankel function of the second kind of zero order and r_i^p is given by

$$r_i^p = \sqrt{(x - x_i^p)^2 + (z - z_i^p)^2}. \tag{32}$$

In (30)

$$H_{ix}^P = \frac{k_p I_i^p (z - z_i^p)}{4jr_i^p} H_1^{(2)}(k_p r_i^p) \tag{33}$$

and

$$H_{iz}^P = \frac{k_p I_i^p (x_i^p - x)}{4jr_i^p} H_1^{(2)}(k_p r_i^p) \tag{34}$$

are the x and z components of the magnetic field at observation point (x, z) in region p due to current filament I_i^p situated at (x_i^p, z_i^p). Here, $H_1^{(2)}$ is the Hankel function of the second kind of first order.

D. Evaluation of the Unknown Currents $\{I_i^w\}$ and $\{I_i^p\}$

Following the procedure outlined toward the end of Section III, we reduce the functional conditions (1) and (2) to a matrix form in which the various matrices are interpreted in terms of generalized network parameters. The result is

$$[Z]\vec{I}=\vec{V} \tag{35}$$

where

$$[Z]=\begin{bmatrix}[Z_e^w] & [Z_e^p]\\ [Z_h^w] & [Z_h^p]\end{bmatrix} \tag{36}$$

$$\vec{I}=\begin{bmatrix}\vec{I}^w\\ \vec{I}^p\end{bmatrix} \tag{37}$$

$$\vec{V}=\begin{bmatrix}\vec{V}_e\\ \vec{V}_h\end{bmatrix}. \tag{38}$$

$[Z]$ is a $2N^s$ by (N^w+N^p) matrix called the generalized impedance matrix, $\vec{I}$ is an (N^w+N^p)-element column vector called the generalized unknown current vector, and $\vec{V}$ is an $2N^s$-element column vector called the generalized voltage source vector. In (36), $[Z_e^w]$ is an N^s by N^w matrix whose (l,i) element is the electric-field intensity E_{iy}^w due to a filament I_i^w of unit current evaluated at (x_l, z_l) on S. Similarly, $[Z_e^p]$ is an N^s by N^p matrix whose (l,i) element is the negative of the electric-field intensity E_{iy}^p due to a filament I_i^p of unit current evaluated at (x_l, z_l) on S. The matrix $[Z_h^w]$ is an N^s by N^w matrix whose (l,i) element is the tangential magnetic-field intensity due to a filament I_i^w of unit current evaluated at (x_l, z_l) on S. Similarly, $[Z_h^p]$ is an N^s by N^p matrix whose (l,i) element is the negative of the tangential magnetic-field intensity due to a filament I_i^p of unit current evaluated at (x_l, z_l) on S. In (37), $\vec{I}^w$ is an N^w-element column vector whose ith element is I_i^w. Similarly, $\vec{I}^p$ is an N^p-element column vector whose ith element is I_i^p. Finally, in (38), $\vec{V}_e$ and $\vec{V}_h$ are N^s-element column vectors whose lth elements are, respectively, the negative of E_y^{inc} and the negative of the tangential magnetic-field intensity at observation point (x_l, z_l) on S.

Having formulated the matrix equation (35), the unknown current vector $\vec{I}$ can be solved for in a straightforward manner. If the boundary conditions are forced at $N^s=\frac{1}{2}(N^w+N^p)$ selected points on S, then $[Z]$ is usually one-to-one and onto.[1] In this case, $[Z]$ is invertible and the unique solution to (35) is readily given by

$$\vec{I}=[Z]^{-1}\vec{V} \tag{39}$$

where $[Z]^{-1}$ is the inverse of matrix $[Z]$. If, on the other hand, the boundary conditions are forced at $N^s>\frac{1}{2}(N^w+N^p)$ selected points on S, then $[Z]$ is usually one-to-one but not onto.[1]

In this case, unless $\vec{V}$ is in the range $[Z]$, there is no exact solution to (35). If $\vec{V}$ is not in the range of $[Z]$, we pursue the smallest least-square-error solution to (35), that is, the one which minimizes the standard norm of the vector $[Z]\vec{I}-\vec{V}$. This solution of (35) is known to be

$$\vec{I}=([\tilde{Z}]^*[Z])^{-1}[\tilde{Z}]^*\vec{V} \tag{40}$$

where the matrix $([\tilde{Z}]^*[Z])^{-1}[\tilde{Z}]^*$ is the pseudoinverse of the matrix $[Z]$. Here, $[\tilde{Z}]$ is the transpose of $[Z]$ and the asterisk denotes complex conjugate.

E. Scattering Matrix and Equivalent Circuit

Once the unknown current vector is derived from either (39) or (40), one can readily proceed to evaluate the scattering matrix $[S^p]$ for terminal planes $z=0^-$ and $z=0^+$, which constitute the post two-port junction. For this purpose, consider two reference planes T_1 and T_2 placed, respectively, on $z=z_{T_1}$, $z_{T_1}<\min\{z|z\in S\}$; $z=z_{T_2}$, $z_{T_2}>\max\{z|z\in S\}$. Assume also that T_1 and T_2 are sufficiently distant from the post surface so that contributions of nonpropagating modes to the fields there may be neglected altogether. Further, assume that the distance to each of the planes from the $z=0$ plane is an integral multiple of the guide wavelength. In accordance with this choice, the scattering matrix for planes T_1 and T_2 becomes identical to $[S^p]$. Hence, the elements S_{11}^p and S_{21}^p of the latter are derivable in term of the following defining equations:

$$S_{11}^p=\frac{E_y^s|_{T_1}}{E_y^{\text{inc}}|_{T_1}} \tag{41}$$

$$S_{21}^p=\frac{\left(E_y^{\text{inc}}+E_y^s\right)|_{T_2}}{E_y^{\text{inc}}|_{T_2}} \tag{42}$$

where $E_y^{\text{inc}}|_{T_1}$ and $E_y^{\text{inc}}|_{T_2}$ are, respectively, the incident electric-field intensities at planes T_1 and T_2, and $E_y^s|_{T_1}$ and $E_y^s|_{T_2}$ are, respectively, the intensities of the y-directed scattered electric field at planes T_1 and T_2.

To evaluate $E_y^{\text{inc}}|_{T_1}$ and $E_y^{\text{inc}}|_{T_2}$, one simply applies (5) to planes T_1 and T_2, obtaining

$$E_y^{\text{inc}}|_{T_1}=\sin\frac{\pi x}{a} \tag{43}$$

$$E_y^{\text{inc}}|_{T_2}=\sin\frac{\pi x}{a}. \tag{44}$$

To compute $E_y^s|_{T_1}$ and $E_y^s|_{T_2}$, one can employ two alternative but, in a sense, equivalent schemes. One option is to simply evaluate the scattered electric field by applying (9) to T_1 and T_2 while retaining only dominant-mode contributions. The result is

$$E_y^s|_{T_1}=\sum_{i=1}^{N^w}-\frac{k_w\eta_w I_i^w}{k_{z1}a}\sin\frac{\pi x_i^w}{a}\sin\frac{\pi x}{a}e^{-jk_{z1}z_i^w} \tag{45}$$

$$E_y^s|_{T_2}=\sum_{i=1}^{N^w}-\frac{k_w\eta_w I_i^w}{k_{z1}a}\sin\frac{\pi x_i^w}{a}\sin\frac{\pi x}{a}e^{jk_{z1}z_i^w}. \tag{46}$$

The other option is to first calculate the total electric field in the post region by (29), which determines the polarization current density $\boldsymbol{J}^{\text{pol}}$ within the dielectric body accord-

[1] $[Z]$ is one-to-one if $[Z]$ does not assign more than one vector $\vec{I}$ in the domain of $[Z]$ to a single vector $\vec{V}$ in the range of $[Z]$ $[Z]$ is onto if every vector $\vec{V}$ in the range of $[Z]$ is associated with at least one vector $\vec{I}$ in the domain of $[Z]$.

ing to

$$\boldsymbol{J}^{\mathrm{pol}} = \boldsymbol{u}_y J^{\mathrm{pol}} = j\omega(\epsilon_p - \epsilon_w)\boldsymbol{E}^p. \tag{47}$$

Treating this polarization current as a source current in a homogeneous waveguide region which generates the scattered field and applying the result to T_1 and T_2 while retaining only dominant-mode contributions, we obtain

$$E_y^s|_{T_1} = -\frac{k_w\eta_w \sin\frac{\pi x}{a}}{k_{z1}a}\iint_{\substack{\text{post}\\ \text{cross section}}} J^{\mathrm{pol}}(x', z') \cdot \sin\frac{\pi x'}{a} e^{-jk_{z1}z'}\,dx'\,dz' \tag{48}$$

$$E_y^s|_{T_2} = -\frac{k_w\eta_w \sin\frac{\pi x}{a}}{k_{z1}a}\iint_{\substack{\text{post}\\ \text{cross section}}} J^{\mathrm{pol}}(x', z') \cdot \sin\frac{\pi x'}{a} e^{jk_{z1}z'}\,dx'\,dz'. \tag{49}$$

We turn to the remaining elements of the scattering matrix. In most practical situations the junction is reciprocal and therefore $S_{12}^p = S_{21}^p$. To determine S_{22}^p, one can construct a new situation by rotating the post by 180° around the x-axis and then evaluate S_{11}^p according to the preceding procedure. Now, S_{11}^p in this new situation is identical to S_{22}^p of the original situation. In many cases, however, there is no need whatsoever to repeat the moment procedure in order to calculate S_{22}^p. In these cases, S_{22}^p is readily expressible in terms of S_{11}^p and S_{21}^p. For a post symmetric with respect to the $z = 0$ plane, S_{22}^p is clearly equal to S_{11}^p. For a lossless junction, $[S^p]$ is a unitary matrix, that is

$$[S^p]^{-1} = [\tilde{S}^p]^* \tag{50}$$

or explicitly

$$|S_{11}^p|^2 + |S_{21}^p|^2 = 1 \tag{51}$$

$$|S_{22}^p|^2 + |S_{21}^p|^2 = 1 \tag{52}$$

and

$$S_{11}^p S_{21}^{p*} + S_{21}^p S_{22}^{p*} = 0. \tag{53}$$

In view of (53), we find that

$$S_{22}^p = -\frac{S_{11}^{p*} S_{21}^p}{S_{21}^{p*}}. \tag{54}$$

A knowledge of the scattering matrix $[S^p]$ permits a rather straightforward calculation of its corresponding impedance matrix $[Z^p]$. The relation between the two matrices is

$$\frac{1}{Z_0}[Z^p] = -([S^p] + [U])([S^p] - [U])^{-1} \tag{55}$$

where $[U]$ is the unit matrix and $Z_0 = k_w\eta_w/k_{z1}$ is the characteristic impedance of the propagating TE_{10} mode. As a matter of convention, this impedance matrix is presented by the lumped T-network shown in Fig. 4. Note

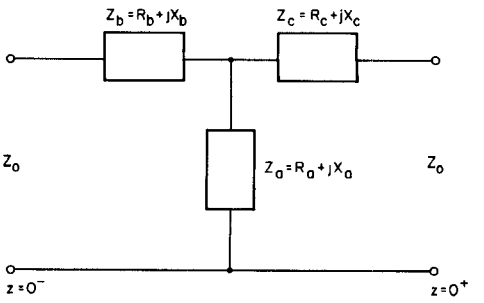

Fig. 4. Typical equivalent circuit for the inductive post discontinuity.

that if the post is symmetric with respect to the $z = 0$ plane we have

$$Z_c = Z_b. \tag{56}$$

V. Numerical Results

Computer programs have been prepared to carry out the analysis of the preceding sections. Listings are included in [10]. The programs are general in that inductive posts of arbitrary shape, location, and complex permittivity can be handled.

To check the program, we consider the few cases for which data are available. Hence, we focus our attention on the case of a circular dielectric post of diameter denoted by d (radius denoted by r) centered at $(x, z) = (a/2, 0)$ in a hollow $(\mu_w = \mu_0, \epsilon_w = \epsilon_0)$ waveguide, which has been treated by Marcuvitz [2], Nielsen [3], and recently by Araneta *et al.* [4] and Sahalos and Vafiadis [5]. Another means of error estimation is available if it is stipulated that the post is lossless. In this case, $[S^p]$ is a unitary matrix and conditions (51) through (53) must be satisfied simultaneously. Finally, a few limiting cases are considered and the degeneration of the results to the proper values is confirmed.

We stated earlier that if the boundary conditions (1) and (2) are satisfied by the Maxwellian and source-free (in their respective regions) fields $(\boldsymbol{E}^w, \boldsymbol{H}^w)$ and $(\boldsymbol{E}^p, \boldsymbol{H}^p)$, then these fields are the true fields. Here, however, we force these conditions to be obeyed only at a finite number of selected points on the common boundary between regions W and P. Naturally, one can question the behavior of the fields on the boundary between the matching point. This is because they can in general be quite different from what is required by the boundary conditions, thereby rendering the results for the field values in the two regions inaccurate. To address this question, we carry out a study of the convergence of the boundary condition errors ΔE and ΔH defined by

$$\Delta E = \frac{|\hat{\boldsymbol{n}} \times (\boldsymbol{E}^w + \boldsymbol{E}^{\mathrm{inc}} - \boldsymbol{E}^p)|_{\mathrm{on}\,S}}{|\boldsymbol{E}^{\mathrm{inc}}|_{\max}} \tag{57}$$

$$\Delta H = \frac{|\hat{\boldsymbol{n}} \times (\boldsymbol{H}^w + \boldsymbol{H}^{\mathrm{inc}} - \boldsymbol{H}^p)|_{\mathrm{on}\,S}}{|\boldsymbol{H}^{\mathrm{inc}}|_{\max}} \tag{58}$$

as a function of the azimuthal angle ϕ for a centered post of $\epsilon_p = 4\epsilon_0$, $d/a = 0.2$, and $a = \lambda/1.4$. We examine the

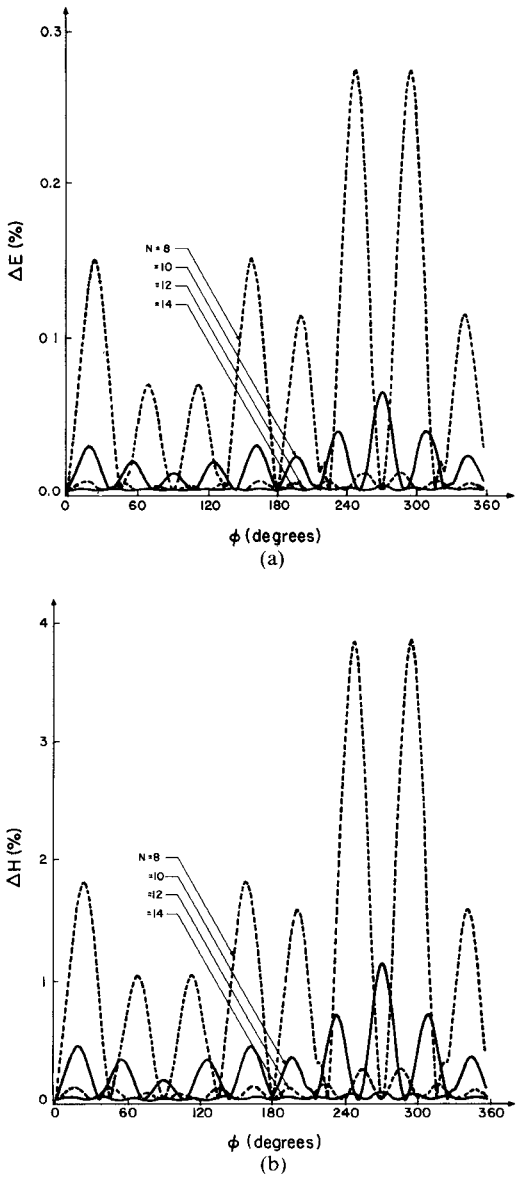

Fig. 5. (a) Boundary condition error ΔE versus ϕ for a centered circular post ($\epsilon_p = 4\epsilon_0$, $d/a = 0.2$, $a = \lambda/1.4$) for various numbers of sources and matching points N. (b) Boundary condition error ΔH versus ϕ for a centered circular post ($\epsilon_p = 4\epsilon_0$, $d/a = 0.2$, $a = \lambda/1.4$) for various numbers of sources and matching points N.

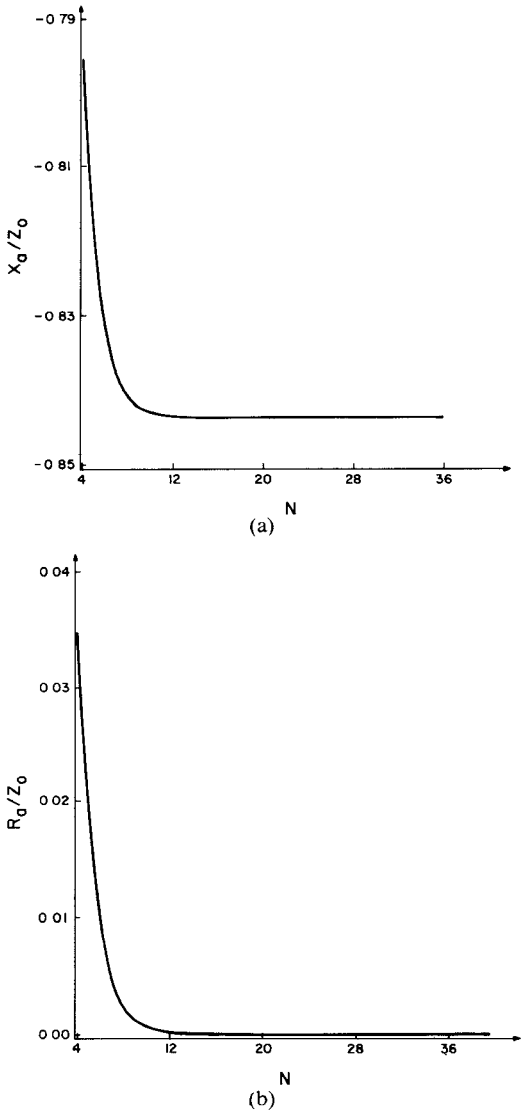

Fig. 6. (a) Normalized reactance X_a/Z_0 versus the number of sources and matching points N for a centered post ($\epsilon_p = 4\epsilon_0$, $d/a = 0.2$, $a = \lambda/1.4$). (b) Normalized resistance R_a/Z_0 versus the number of sources and matching points N for a centered post ($\epsilon_p = 4\epsilon_0$, $d/a = 0.2$, $a = \lambda/1.4$).

special choice of an equal number of inner sources N^w, outer sources N^p, and matching points N^s. We denote this common number by N. The inner sources $\{I_i^w\}$ are placed on a circular surface of radius $r_s^w = 0.5r$ and the outer sources $\{I_i^p\}$ are placed on a circular surface of radius $r_s^p = 2r$. Both the sources and the matching points are evenly spaced on their respective surfaces. The angle ϕ here is the azimuthal angle in an auxiliary cylindrical coordinate system with a z axis coinciding with the post axis and an x axis coinciding with the x axis in Fig. 1. Hence, the interval from 0° to 180° on ϕ is in the "shadow" region of the post surface, while the interval from 180° to 360° on ϕ is in the illuminated region. Plots of ΔE and ΔH for various values of the parameter N are presented in Fig. 5. Cases considered are $N = 8$, 10, 12, and 14. The boundary condition errors ΔE and ΔH which, by conditions (1) and (2), are zero at the matching points increase smoothly and reach a maximum on the surface S between the points. As the number of matching points increases, the maxima of ΔE and ΔH on the surface fall sharply. Note that even for N as small as 14, the maximum of ΔH, which is much larger than the maximum of ΔE, is smaller than 0.1 percent. The nature of convergence seen here is similar in other cases involving posts of other radii and permittivities and in cases where the sources are placed on other surfaces. The rate of convergence, though, may be different. To give some additional information on the convergence as the number of expansion functions and matching points is increased, Fig. 6 depicts plots of the normalized reactance X_a/Z_0 and the normalized resistance R_a/Z_0 versus N for the post of Fig. 5. Note that here for N as small as 14, the numerical solution for X_a/Z_0 converges to an adequate engineering solution, while the solution for R_a/Z_0 converges appropriately to zero, as expected in this lossless case. The rate of convergence is similar for the plots of X_b/Z_0 and R_b/Z_0, which

are not shown here, and of a similar nature in other cases as well.

The choice of the filamentary sources location may also affect the rate of convergence. Studies have shown that the results converge faster to a limiting value when the sources are situated on contours concentric with S and of figures similar to S. For the circular post, this implies that the set $\{I_i^w\}$ is placed on a circular surface of radius r_s^w, while the set $\{I_i^p\}$ is placed on a circular surface of radius r_s^p. In addition, it is found that any selection of r_s^w between $0.2r$ and $0.8r$ and of r_s^p greater than 1.5 virtually does not affect the rate of convergence. In contrast, the rate of convergence deteriorates when the inner sources approach either the post center or the post surface, and when the outer sources approach the post surface.

So far, we brought up cases in which the two continuity conditions (1) and (2) are strictly imposed at the matching points on S. Another option attempted was to impose these conditions in the least-square-error sense at selected points on S with a view to obtaining similar accuracies using fewer sources, thereby gaining the advantage of inverting smaller matrices. For example, the same accuracy stabilized with $N = N^p = 14$ sources, and $N^s = 14$ matching points in a strict solution of the post of the previous case is stabilized with $N^w = N^p = 12$ sources and $N^s = 16$ matching points in a least-square-error solution. Notice that while the former requires an inversion of a 28×28 matrix, the latter requires only an inversion of a 24×24 matrix.

In summary, it should be apparent that it is impossible to state a rule of thumb as to the choice of the source's location and number, since the number of parameters involved is very large. However, it is evident and understandable that a large post of high permittivity will naturally require more sources than a smaller one of lower permittivity in order to achieve the same level of accuracy. We wish to emphasize that even for choices less than optimal in the source's location, the solution eventually converges to the appropriate limiting values as the number of sources and matching points increases. This convergence might, however, be less rapid compared with other choices. Clearly, in any event one should test the solution by increasing the number of sources and matching points and comparing the results. If the results are sufficiently close, the solution is taken as satisfactory. Attention should also be recalled to the summations in (14), (23), and (24). As a practical necessity, a truncation of these infinite series is required. With this in mind, the program divides each series into ten-term sets and subsequently sums up these sets as long as the ratio between the sum of the last ten-term set and the total sum of all the sets considered up to that point is larger than a suitably prescribed threshold. As stated earlier, the resultant error can be quantitatively estimated, in the loss-free case, from the unitary conditions (51)–(53). Finally, with regard to the two options (45), (46) and (48), (49) mentioned to compute E_y^s, studies have shown that they give identical results. For the final results presented in this paper, we favor the simpler one and compute E_y^s using (45), (46).

TABLE I
COMPARISON BETWEEN COMPUTED NORMALIZED REACTANCES X_a/Z_0 AND X_b/Z_0 VERSUS $\sqrt{\epsilon_p/\epsilon_0}$ AND MARCUVITZ'S DATA FOR A CENTERED POST ($d/a = 0.1$, $a = \lambda/1.4$)

	Marcuvitz's data Reference [2]		Our results	
$\sqrt{\frac{\epsilon_p}{\epsilon_0}}$	$\frac{X_a}{Z_0}$	$\frac{X_b}{Z_0}$	$\frac{X_a}{Z_0}$	$\frac{X_b}{Z_0}$
2	-3 12	0 00093	-3.187	0.000968
3	- 1 03	0 00262	- 1.050	0 00270
4	-0 438	0 0053	-0.452	0 00543
5	-0 187	0.0092	-0 196	0.00957
6	-0 057	0.0153	-0.0634	0.0159
7	0.028	0.0249	0.0132	0.0263
8	0.063	0.042	0 0577	0 0452
9	0.083	0.078	0 0743	0 0891
10	0.05	0.21	0.00185	0.294
11	0 6	- 0.87	0.378	-0 409
12	0.3	-0 17	0 269	-0.143
13	0 28	-0.11	0 270	-0.0941
14	0 29	-0.079	0.292	-0 0732
15	0.34	-0.066	0.340	-0.0614

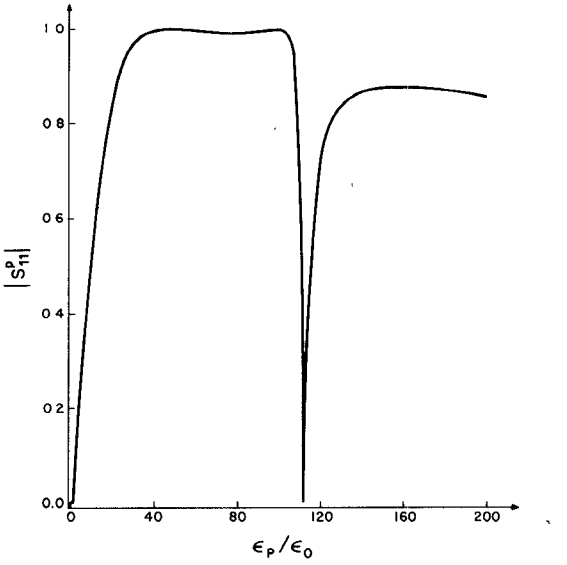

Fig. 7. Reflection coefficient magnitude $|S_{11}^p|$ versus ϵ_p/ϵ_0 for a centered post ($d/a = 0.1$, $a = \lambda/1.4$).

In view of the large number of parameters involved in the general procedure, we will limit the data display to only a few illustrative examples. A comparison between our computed normalized reactances X_a/Z_0 and X_b/Z_0 versus $\sqrt{\epsilon_p/\epsilon_0}$, and Marcuvitz's data [2] for $d/a = 0.1$ and $a = \lambda/1.4$ is presented in Table I. As expected, the results agree with each other fairly well for many values of $\sqrt{\epsilon_p/\epsilon_0}$ but differ significantly in cases where X_b/Z_0 is close to resonance, for which Marcuvitz's results, as pointed out by Marcuvitz himself, do not apply. The behavior of the corresponding reflection coefficient for this case has been recently investigated by Sahalos and Vafiadis [5], who compared their data with those of Marcuvitz [2], Nielsen [3], and Araneta *et al.* [4]. It is observed from Fig. 4 of [5] that the various results agree with each other in many regions but appear to be different near the resonance. Our computed results, depicted in Fig. 7, concur with Sahalos

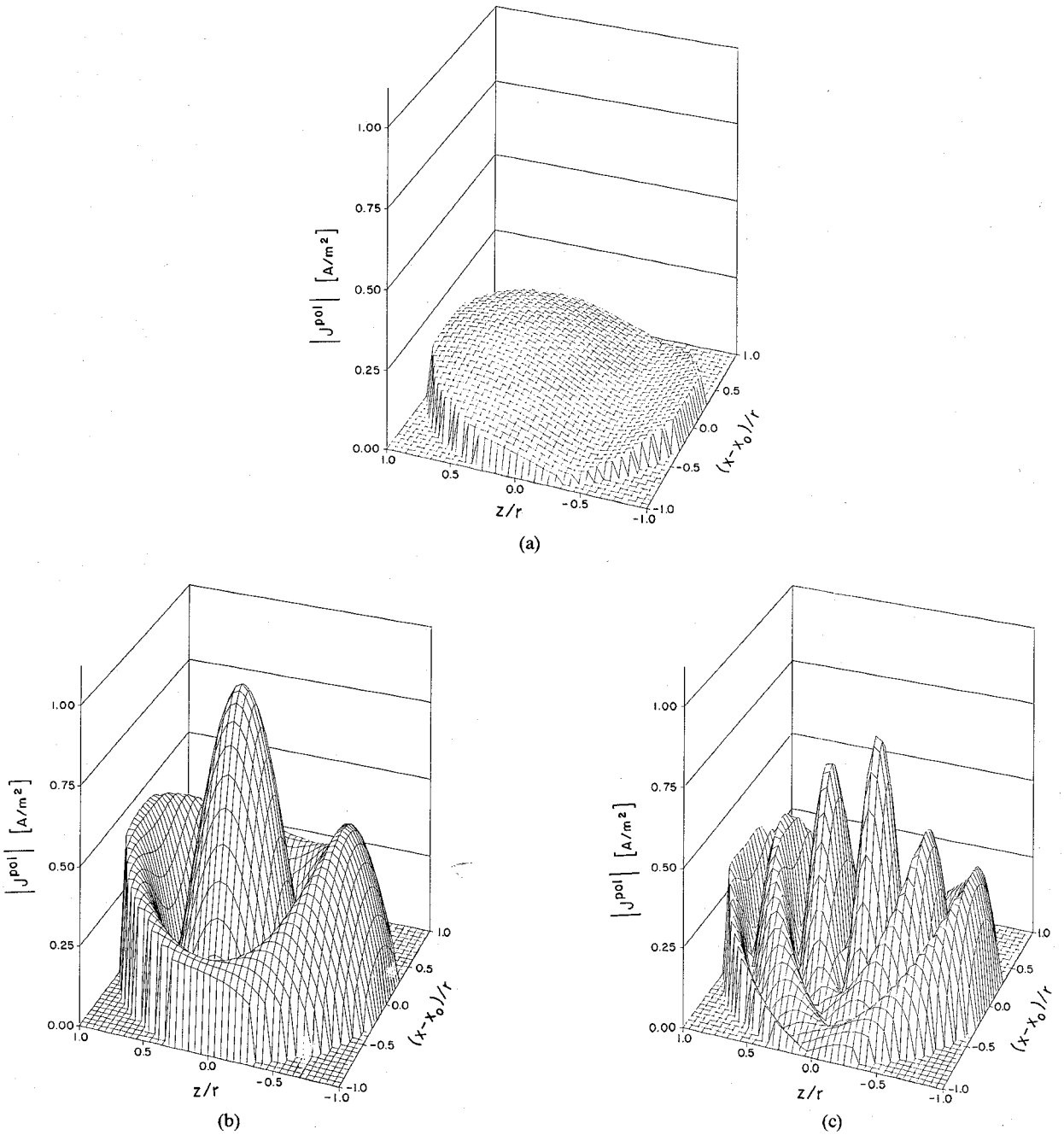

Fig. 8. (a) Three-dimensional picture of the polarization current distribution induced in a centered dielectric post of radius $r = 0.1a$, $a = \lambda/1.4$, and permittivity $\epsilon_p = 10\epsilon_0$. (b) Three-dimensional picture of the polarization current distribution induced in a centered dielectric post of radius $r = 0.1a$, $a = \lambda/1.4$, and permittivity $\epsilon_p = 100\epsilon_0$. (c) Three-dimensional picture of the polarization current distribution induced in a centered dielectric post of radius $r = 0.2a$, $a = \lambda/1.4$, and permittivity $\epsilon_p = 100\epsilon_0$.

and Vafiadis's data. Our numerical procedure also shows the resonant condition at a dielectric constant of $\epsilon_p = 112.5\epsilon_0$. It should be emphasized that our method is apparently more powerful since it is not limited to the case of a circular centered post but is rather general in that posts of arbitrary smooth shape, size, location, and number can be handled effectively.

Another parameter of interest is the polarization current distribution within the dielectric post. This current can be readily evaluated via (47) once the electric field $\boldsymbol{E}^p$ due to the current filaments I_i^p, $i = 1, 2, \cdots, N^p$, is known. Illustrative three-dimensional pictures of the magnitude of J^{pol} for various cases are shown in Fig. 8. It should be emphasized that the convergence of the results for the field values in each region to their limiting values as the number of sources and matching points is increased is similar to the convergence of the boundary condition errors to zero. In the results for the polarization current calculated from the field value in region P, the limiting value is reached within less than 0.1-percent error. Note that the polarization current intensity varies in magnitude and that these variations become appreciable as the post gets thicker and

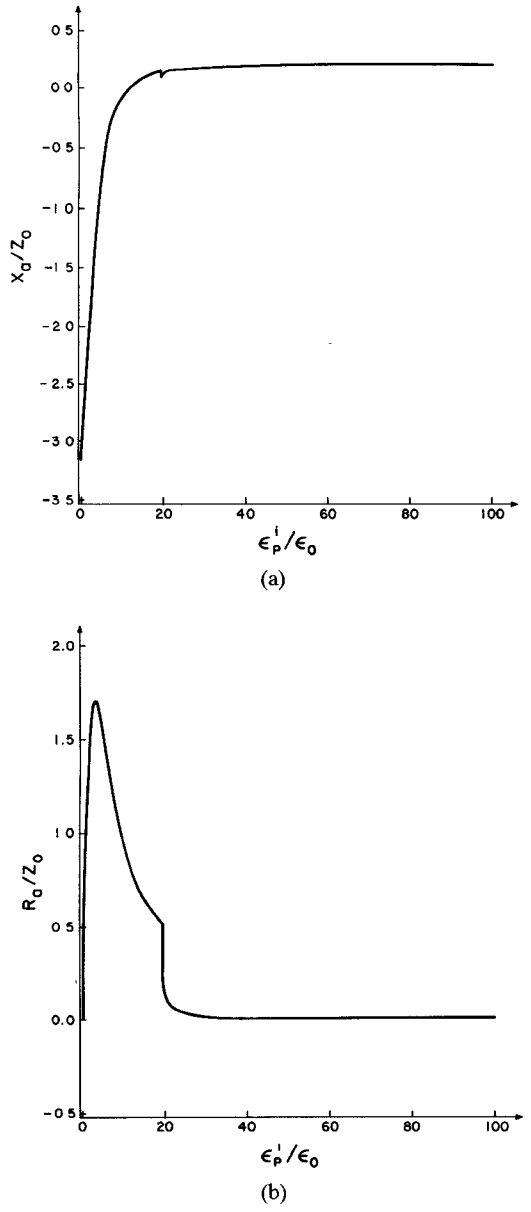

Fig. 9. (a) Normalized reactance X_a/Z_0 versus ϵ_p^i/ϵ_0 for a centered lossy post ($\epsilon_p^r = 4\epsilon_0$, $a = \lambda/1.4$). (b) Normalized resistance R_a/Z_0 versus ϵ_p^i/ϵ_0 for a centered lossy post ($\epsilon_p^r = 4\epsilon_0$, $a = \lambda/1.4$).

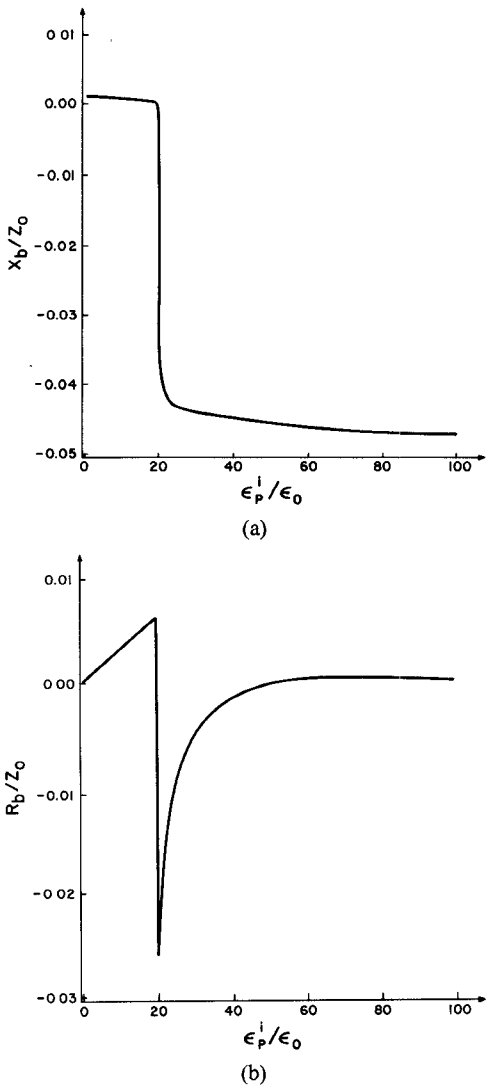

Fig. 10. (a) Normalized reactance X_b/Z_0 versus ϵ_p^i/ϵ_0 for a centered lossy post ($\epsilon_p^r = 4\epsilon_0$, $a = \lambda/1.4$). (b) Normalized resistance R_b/Z_0 versus ϵ_p^i/ϵ_0 for a centered lossy post ($\epsilon_p^r = 4\epsilon_0$, $a = \lambda/1.4$).

as its permittivity becomes higher. This behavior is due to the variation of the electric-field intensity in the dielectric region to which J^{pol} is related through (47). The variation of the electric field in the dielectric region is not surprising as it can be found in similar but nevertheless different situations involving scattering by dielectric cylinders [11], [12]. Thus, poor accuracy is to be expected if the polarization current is calculated approximating the electric field in the dielectric by the slowly varying field of the incident TE_{10} mode. Obviously, if the fields scattered by the post are computed from these current distributions as source currents and from the inner filamentary currents as source currents, virtually identical results are obtained.

Lossy dielectric posts are handled by the use of complex permittivities. Hence, we let $\epsilon_p = \epsilon_p^r - j\epsilon_p^i$ with ϵ_p^r and ϵ_p^i real. Figs. 9 and 10 show, respectively, plots of normalized reactances X_a/Z_0 and X_b/Z_0 and resistances R_a/Z_0 and R_b/Z_0 as a function of ϵ_p^i for centered post of $d/a = 0.1$, with $\epsilon_p^r = 4\epsilon_0$ at $\lambda/a = 1.4$. Note that in the two limiting cases, namely, $\epsilon_p^i \to 0$ and $\epsilon_p^i \to \infty$, the results for the lossless post shown in Table I and for the perfectly conducting post given in [7] are, respectively, recovered. Fig. 11 exhibits the variation of the left-hand side of (51) as a function of ϵ_p^i for the lossy post. The graph shows that in the two above-mentioned limiting cases, the value 1 is approached in accordance with the power conservation law that must be satisfied in these particular instances. Observe that in this situation post losses appear to have reached a peak value at $\epsilon_p^i = 19.5\epsilon_0$. Notice also the abrupt change in the magnitude of each of the reactances and resistances of Figs. 9 and 10 that occurs at $\epsilon_p^i = 19.5\epsilon_0$, which results in the sharp falloff in post losses seen in Fig. 11.

The extension of the preceding formulation to encompass cases involving multiple-post, say M, obstacles is straightforward. In these cases, the field in the waveguide

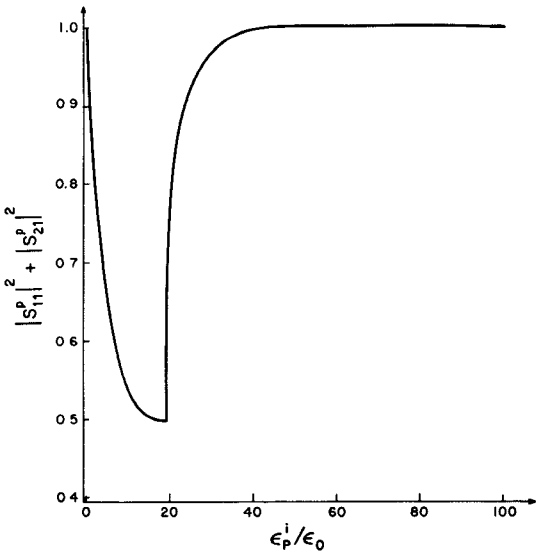

Fig. 11. Power balance versus ϵ^i_p/ϵ_0 for a centered lossy post ($\epsilon^r_p = 4\epsilon_0$, $a = \lambda/1.4$).

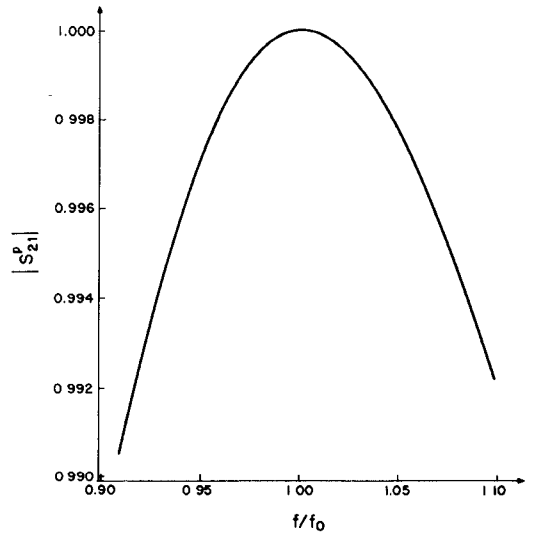

Fig. 12. Transmission coefficient versus frequency for a two-element centered dielectric post configuration ($\epsilon_p = 4\epsilon_0$, $d/a = 0.1$, $a = \lambda/1.4$).

is simulated by the field of M sets of sources, each situated inside its corresponding post. The field inside each post is simulated, as before, by the field of an appropriate set situated outside that post. Boundary conditions must be subsequently applied at selected points on the M post surfaces. Fig. 12 shows computed transmission coefficient data for a two-element centered dielectric post ($\lambda/a = 1.4$, $d/a = 0.1$, $\epsilon_p = 4\epsilon_0$) as a function of frequency. Here, the spacing between the post axes along the z direction has been determined to yield resonance (complete transmission) at f_0 neglecting the higher order mode interactions between posts, that is, obtained by cascading single-post equivalent circuits. The curve, however, corresponds to results obtained, including high-mode interactions as well. Observe that there is no appreciable difference between the resonance location in the curve and the computed one. This is due to the fact that in the case shown we are dealing with thin posts of relatively low permittivity; thus, higher order mode interactions may be neglected. In other cases, however, such as thick posts of high permittivity which render the frequency response high Q, the higher modes must be accounted for.

VI. Discussion

A complete analysis of dielectric post structures of the inductive type in rectangular waveguides has been facilitated via a simple, accurate, rapidly converging moment procedure. The solution uses one set of filamentary currents to simulate the field scattered by the post, another set to simulate the diffracted field inside the post, and a testing procedure for imposing the continuity conditions for the tangential components across the post surface. The procedure is general in that inductive dielectric posts of arbitrary smooth shape, size, location, and number can be handled effectively. Lossy posts have also been considered.

The computed results show very good agreement with Sahalos and Vafiadis's data. They also give proper results in several limiting cases. In the absence of the dielectric post ($\epsilon_p = \epsilon_w$), S^p_{11} and S^p_{21} approach, respectively, the correct values 0 and 1. Also, as $\mathrm{Im}(\epsilon_p) \to -\infty$, the results of [7] for the perfectly conducting post are recovered. The advantage of our method over the previously suggested ones is its generality. While these methods are applicable to a single centered post of circular cross section, our method can handle an array of any number of posts, lossless as well as lossy, of arbitrary smooth shape and location.

The accuracies achievable by this theoretical model are indeed excellent with respect to engineering needs. The suggested procedure is applicable to a variety of microwave dielectric discontinuities of the inductive type and can thus prove useful in the analysis and synthesis of waveguide components built of newly developed ceramic compositions.

An extension to encompass dielectric discontinuities of the dual-capacitive type requires changes but appears to be straightforward. Since each post is uniform along the x axis, and since the exciting mode has an x component of magnetic field that varies as $\sin(\pi x/a)$ and no x component of electric field, only TE_{1n} to x modes will be excited in the waveguide. Thus, one can readily use sets of x-directed magnetic current filaments that vary as $\sin(\pi x/a)$ to simulate the fields scattered by the post and the field inside the post, and subsequently match the boundary conditions in some $x =$ constant plane within the waveguide.

References

[1] P. G. Li, A. T. Adams, Y. Leviatan, and J. Perini, "Multiple-post inductive obstacle in rectangular waveguide," *IEEE Trans. Microwave Theory Tech.*, vol. MTT-32, pp. 365–373, Apr. 1984.

[2] N. Marcuvitz, Ed., *Waveguide Handbook* (M.I.T. Rad. Lab. Ser., vol. 10). New York: McGraw-Hill, 1951.

[3] E. D. Nielsen, "Scattering by a cylindrical post of complex permittivity in a waveguide," *IEEE Trans. Microwave Theory Tech.*, vol. MTT-17, pp. 148–153, Mar. 1969.

[4] J. A. Araneta, M. E. Brodwin, and G. A. Kriegsmann, "High-temperature microwave characterization of dielectric rods," *IEEE Trans. Microwave Theory Tech.*, vol. MTT-32, pp. 1328–1335, Oct. 1984.
[5] J. N. Sahalos and E. Vafiadis, "On the narrow-band microwave filter design using a dielectric rod," *IEEE Trans. Microwave Theory Tech.*, vol. MTT-33, pp. 1165–1171, Nov. 1985.
[6] J. K. Plourde and C. Ren, "Applications of dielectric resonators in microwave components," *IEEE Trans. Microwave Theory Tech.*, vol. MTT-29, pp. 754–770, Aug. 1981.
[7] Y. Leviatan, P. G. Li, A. T. Adams, and J. Perini, "Single-post inductive obstacle in rectangular waveguide," *IEEE Trans. Microwave Theory Tech.*, vol. MTT-31, pp. 806–811, Oct. 1983.
[8] Y. Leviatan, D. Shau, and A. T. Adams, "Numerical study of the current distribution on a post in a rectangular waveguide," *IEEE Trans. Microwave Theory Tech.*, vol. MTT-32, pp. 1411–1415, Oct. 1984.
[9] C. G. Hsu and H. A. Auda, "Multiple dielectric posts in a rectangular waveguide," private communication.
[10] Y. Leviatan and G. S. Sheaffer, "Analysis of inductive dielectric posts in rectangular waveguide," EE Pub. No. 544, Dept. of Elect. Eng., Technion—Israel Institute of Technology, Haifa, Israel, Nov. 1985.
[11] J. H. Richmond, "Scattering by a dielectric cylinder of arbitrary cross-section shape," *IEEE Trans. Antennas Propagat.*, vol. AP-13, pp. 334–341, May 1965.
[12] R. F. Harrington, *Time-Harmonic Electromagnetic Fields*. New York: McGraw-Hill, 1961, p. 261.

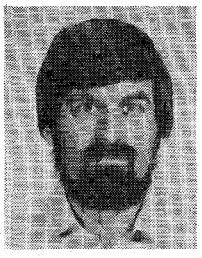

Yehuda Leviatan (S'81–M'82) was born in Jerusalem, Israel, on September 19, 1951. He received the B.Sc. and M.Sc. degrees in electrical engineering from the Technion—Israel Institute of Technology, Haifa, Israel, in 1977 and 1979, respectively, and the Ph.D. degree in electrical engineering from Syracuse University, Syracuse, NY, in 1982.

He held a Teaching Assistantship during his graduate work from 1977 to 1979 at the Technion, a Research Assistantship during his graduate work from 1979 to 1981 at Syracuse University, and a Postdoctoral Research position at Syracuse University during the summer of 1982. From 1980 to 1982, he also was engaged as a part-time Research Engineer at the Syracuse Research Corporation. During the 1982/83 academic year, he was with the Faculty of the Electrical and Computer Engineering Department at Syracuse University as an Assistant Professor. He has provided consulting services to the Syracuse Research Corporation, IBM (Endicott Laboratory), and to Adaptive Technology, Inc. In October 1983, he joined the Department of Electrical Engineering at the Technion where at present he is a Lecturer. During the summer of 1985, he was a Visiting Assistant Professor with the School of Applied and Engineering Physics, Cornell University. Dr. Leviatan's research interests are in the areas of mathematical and numerical methods applied to antennas, transmission lines, and waveguides, scattering and transmission through apertures, near fields of radiating systems, and adaptive arrays. He has published several journal papers on electromagnetics and presented others at international symposia.

A paper he co-authored has won the third best award at the 1983 IEEE International EMC Symposium. He is a Fellow of the B. De Rothschild Foundation for the Advancement of Science in Israel, Inc.

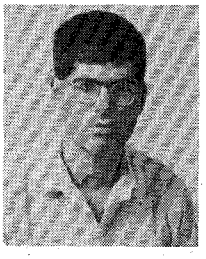

Gad S. Sheaffer was born in Haifa, Israel, on November 17, 1954. He received the B.Sc. and M.Sc. degrees in electrical engineering in 1982 and 1985, respectively, both from the Technion—Israel Institute of Technology, Haifa, Israel.

Since 1983, he has been a Teaching Assistant at the Technion. His current research interests are in developing analytical and numerical techniques for the analysis of waveguide discontinuities.